

Droplet-based vitrification of adherent human induced pluripotent stem cells on alginate microcarrier influenced by adhesion time and matrix elasticity

Ina Meiser^{a,*}, Julia Majer^a, Alisa Katsen-Globa^a, André Schulz^a, Katharina Schmidt^a, Frank Stracke^a, Eirini Koutsouraki^b, Gesa Witt^c, Oliver Keminer^c, Ole Pless^c, John Gardner^b, Carsten Claussen^c, Philip Gribbon^c, Julia C. Neubauer^{a,d,1}, Heiko Zimmermann^{a,b,e,f,1}

^a Fraunhofer Institute for Biomedical Engineering IBMT, 66280, Sulzbach, Saar, Germany

^b Censo Biotechnologies Ltd, Roslin Midlothian, EH25 9RG, United Kingdom

^c Fraunhofer Institute for Translational Medicine and Pharmacology ITMP, ScreeningPort, 22525, Hamburg, Germany

^d Fraunhofer Project Centre for Stem Cell Process Engineering, 97081, Würzburg, Germany

^e Faculty of Marine Science, Universidad Católica Del Norte, 1781421, Coquimbo, Chile

^f Chair for Molecular and Cellular Biotechnology / Nanotechnology, Saarland University, 66123, Saarbrücken, Germany

ARTICLE INFO

Keywords:

Vitrification
Microcarrier
Human induced pluripotent stem cells
Adherent cryopreservation

ABSTRACT

The gold standard in cryopreservation is still conventional slow freezing of single cells or small aggregates in suspension, although major cell loss and limitation to non-specialised cell types in stem cell technology are known drawbacks. The requirement for rapidly available therapeutic and diagnostic cell types is increasing constantly. In the case of human induced pluripotent stem cells (hiPSCs) or their derivatives, more sophisticated cryopreservation protocols are needed to address this demand. These should allow a preservation in their physiological, adherent state, an efficient re-cultivation and upscaling upon thawing towards high-throughput applications in cell therapies or disease modelling in drug discovery. Here, we present a novel vitrification-based method for adherent hiPSCs, designed for automated handling by microfluidic approaches and with ready-to-use potential e.g. in suspension-based bioreactors after thawing. Modifiable alginate microcarriers serve as a growth surface for adherent hiPSCs that were cultured in a suspension-based bioreactor and subsequently cryopreserved via droplet-based vitrification in comparison to conventional slow freezing. Soft (0.35%) versus stiff (0.65%) alginate microcarriers in concert with adhesion time variation have been examined. Findings revealed specific optimal conditions leading to an adhesion time and growth surface (matrix) elasticity dependent hypothesis on cryo-induced damaging regimes for adherent cell types. Deviations from the found optimum parameters give rise to membrane ruptures assessed via SEM and major cell loss after adherent vitrification. Applying the optimal conditions, droplet-based vitrification was superior to conventional slow freezing. A decreased microcarrier stiffness was found to outperform stiffer material regarding cell recovery, whereas the stemness characteristics of rewarmed hiPSCs were preserved.

1. Introduction

Human induced pluripotent stem cells (hiPSCs), reprogrammed from somatic cells, have the potential of unlimited self-renewal and the capacity to differentiate to any cell type of the body [1,2]. Starting from healthy or diseased individuals as donors, hiPSCs serve as a starting point for patient- and disease-specific cells and thus take the field of

regenerative medicine, developmental biology, and diagnostics to the next level [3]. This cutting-edge discovery has enabled disease-specific models for drug screening, e.g. amyotrophic lateral sclerosis [4], retinitis pigmentosa [5] or cardiomyopathies [6], and even curative cell-based therapies to be developed [7,8]. Prominent targets for the latter are ophthalmological diseases, where hiPSC-derived retinal epithelial cell are developed as advanced therapy medical product

* Corresponding author.

E-mail address: ina.meiser@ibmt.fraunhofer.de (I. Meiser).

¹ equal contribution.

<https://doi.org/10.1016/j.cryobiol.2021.09.010>

Received 21 July 2021; Received in revised form 22 September 2021; Accepted 23 September 2021

Available online 25 September 2021

0011-2240/© 2021 The Authors.

Published by Elsevier Inc.

This is an open access article under the CC BY-NC-ND license

(<http://creativecommons.org/licenses/by-nc-nd/4.0/>).

(ATMP) to treat age-related macula degeneration [9]. A basic prerequisite for these broad fields of applications is the sufficient supply of hiPSCs and a robust logistic for hiPSCs and hiPSC-derived ATMPs. Current biotechnological approaches develop protocols and devices for large-scale expansion to secure the supply of undifferentiated hiPSCs [10]. Whereas conventional expansion strategies utilise standard adherent cultivation techniques in manual procedures, novel approaches implement suspension-based bioreactors with higher throughput in concert with the optimization of medium to biomass ratios leading to the possibility for automated on-line monitoring and sample manipulation [11]. Such bioreactors combine the benefits of large scale production with the option to either run the process in the well-known conventional two-dimensional cultivation routine using microcarriers as a growth surface [12] or as three dimensional cell cultures as an optimal starting point for subsequent differentiation processes [13]. However, little progress has been made towards reaching the goal of storing bulk quantities of viable and fully functional cells in an application-oriented manner. Whereas cryopreservation is still the only option to store viable biomaterial for unlimited time, the current cryotechnological infrastructure in biobanks is designed for keeping cell-stocks in relatively small aliquots (e.g. 1 ml cryovials) followed by expansion and cell manipulation routines at the recipient's site to finally achieve the desired cell state and format [14]. The conventional and most commonly used cryopreservation method for hiPSCs is a slow freezing protocol of single cells in suspension applying cooling rates of approx. $-1\text{ }^{\circ}\text{C}/\text{min}$ [15]. Despite the addition of various cryoprotective agents (CPAs), like 10% dimethyl sulfoxide (Me_2SO), thawed hiPSCs show poor re-attachment and recovery rates [16]. Besides the damaging effects caused directly by the formation of ice crystals during freezing which indiscriminately affects any cell type, the sensitivity of hiPSCs to the necessary detachment and dissociation process using enzymatically active agents is a main reason for this reduced viability [17]. The use of Rho/Rho-associated protein kinase (ROCK) inhibitor can support both the dissociation as well as the cryopreservation process by reducing the incidence of dissociation-induced cell death but has been reported to cause unwanted effects [18,19]. Although there are promising approaches to cryopreserving adherent cells by means of conventional slow freezing protocols [20,21,22], application-oriented routines for large-scale cryopreservation are missing especially for sensitive hiPSCs. A second cryopreservation regime, vitrification, enables the maintenance of cells in their adherent state, thus avoiding potentially harmful dissociation steps. With ultra-fast cooling rates and adjusted CPA concentrations within the sample, ice formation and thus damaging mechanisms like osmotic shock, water depletion and mechanical membrane ruptures are avoided [23]. The superiority of vitrification especially for tissue engineered products, has already been demonstrated for encapsulated bone marrow stem cells in alginate-fibrin-beads [24] as well as for adherent mesenchymal stem cells on alginate-beads [25]. However, up until now, vitrification approaches have required skilled handling and are only valid for small sample sizes, making it unsuitable for bulk storage [26,27]. Here we report a novel approach combining the advantages of alginate-based microcarriers with modifiable characteristics for cultivation of hiPSCs together with a vitrification approach. The process was designed for automation, allowing application-oriented large-scale cryopreservation towards ready-to-use storable hiPSCs in suspension-based bioreactors. In addition, the findings presented in this study lead to the hypothesis of an optimal adhesion time prior to cryopreservation dependent on cell type and matrix elasticity.

2. Material and methods

2.1. Cultivation of hiPSC

The human induced pluripotent stem cell line RCi53 (Censo Biotechnologies Ltd, Edinburgh (UK)), was routinely cultured on 0.009 mg protein/cm² growth factor reduced Matrigel (Corning, New York, USA)

coated 60 mm Nunc™ culture plates (Thermo Fisher Scientific, Waltham, USA) and kept at 37 °C in a standard incubator. Cells were cultured in defined basal medium, mTeSR™1 (Stemcell Technologies, Vancouver, Canada) supplemented with Pen-Strep-Glutamine (Thermo Fisher Scientific, Waltham, USA) (1:100), composed of 10 units/ml penicillin, 10 µg/ml streptomycin and 29.2 mg/ml L-glutamine. After thawing, 3 µM ROCK-inhibitor Y-27632 (Abcam, Cambridge, UK) was added for 24 h and replaced with mTeSR™1 afterwards. Detachment of hiPSCs was performed with 0.5 mM EDTA in Phosphate Buffered Saline PBS (without Ca²⁺ and Mg²⁺) (Thermo Fisher Scientific, Waltham, USA) to yield small cell aggregates of approximately 20 µm. Therefore, the hiPSCs were washed with 2 ml EDTA solution and incubated for approx. 5 min at 37 °C in fresh EDTA solution (2 ml). When the hiPSCs appear white in phase contrast microscopy, EDTA solution was removed and cells were detached from the surface by rinsing with mTeSR™1.

2.2. Alginate microcarrier production

Two sources of ultra high viscous alginate were used derived from the brown algae species *Lessonia trabeculata* (LT) and *Lessonia nigrescens* (LN) (originally produced 'in house', now available via Alginatex, Riedenheim, Germany) [28]. Both extracted alginates were dissolved in a 1:1 ratio in 0.9% sodium chloride (NaCl; B. Braun, Melsungen, Germany) to final concentrations of 0.35% and 0.65% (w/v %) to provide microcarriers of different stiffnesses. The microcarrier production was performed as reported before [29]. Following an incubation in BaCl₂ solution for 20 min, microcarriers were collected and washed three times in 0.9% NaCl for 3 min. To provide a suitable growth surface for the hiPSCs, the alginate microcarriers were coated with the standard cultivation matrix Matrigel by aqueous carbodiimide chemistry. This process required activation buffer consisting of 50 mM N-hydroxysuccinimide (NHS; Sigma-Aldrich, St. Louis, USA) and 200 mM N-ethyl-N'-(3-dimethylaminopropyl) carbodiimide hydrochloride (EDC; Merck, Darmstadt, Germany) and was performed as described previously [30].

2.3. Characterization of alginate microcarrier

To quantify microcarrier properties, dynamic mechanical analyses and compression tests were conducted. Therefore, planar alginate layers were produced from both solutions on round standard cell culture treated polystyrene-based coverslips (Thermanox™, Ø 13 mm; Thermo Fisher Scientific, Waltham, USA) that were treated with poly-L-Lysine (PLL; Sigma-Aldrich, St. Louis, USA) in phosphate buffered saline (PBS; Thermo Fisher Scientific, Waltham, USA) for 30 min at 37 °C. The alginate solutions (LN/LT 1:1, 0.35% and 0.65%) were placed on the treated, dried plastic surfaces and gelled with 20 mM BaCl₂ solution for 20 min at room temperature. The obtained alginate layers were washed three times with NaCl. To determine the storage and loss moduli of the respective sol and gelled layer, both alginate samples were subjected to a frequency sweep between 0.1 and 100 s⁻¹. The shear measurements (n = 5) were carried out using the rotational rheometer Physica MCR 101 (Anton Paar, Graz, Austria) with a parallel plate geometry and a Peltier element adjusted at 20 °C. For the compression test, 0.35% and 0.65% alginate gels (Ø 13 mm, height: 1.4 mm) surrounded with NaCl were compressed until 35% of strain with a deformation rate of 0.5 mm/s using TA.XTplus (Stable Micro Systems, Godalming, UK; n = 24). The elastic moduli were calculated as the slope of the stress-strain curve (10–30% of strain, see Suppl. Figure 1).

2.4. hiPSC culture in CERO 3D

The cultivation of hiPSCs on microcarriers in suspension was performed in CERO 3D cell culture system (OLS OMNI Life Science, Bremen, Germany). Alginate microcarriers and cell suspension were added into CEROTubes (OLS OMNI Life Science, Bremen, Germany) and cultured in

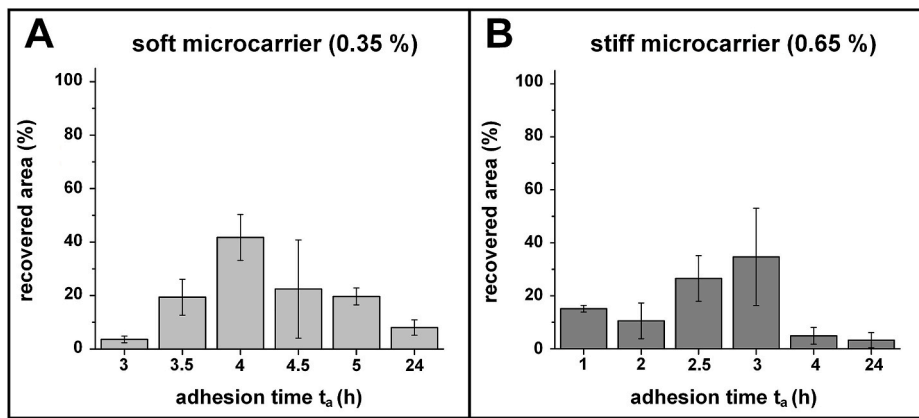


Fig. 1. Recovery of hiPSCs on soft and stiff alginate microcarrier after vitrification.

Recovered area of hiPSCs after vitrification has been detected via image analysis and is shown normalised to the non-frozen control. Prior to vitrification, the hiPSCs were inoculated for $t_a = 3, 3.5, 4, 4.5, 5,$ and 24 h on soft and for $t_a = 1, 2, 2.5, 3, 4,$ and 24 h on stiff alginate microcarrier (biological replicates $N = 3$, technical replicates $n = 8$).

mTeSR™1 for different incubation and attachment times (between 1 and 24 h) in a standard hiPSC culture program. The program comprised inoculation as well as incubation stages and a rotation speed of 40 rpm. Other parameters applied were a direction-changing rotation after 4 s, temperature of 37 °C and a CO₂ concentration of 5%. For each condition and time point, 3×10^5 cells/cm² were inoculated on a total growth surface of 50 cm² for both microcarrier types (soft and stiff). The growth surface per microcarrier was determined by measuring the diameter using the program NIS-Elements (Nikon, Tokyo, Japan) applying the formula $4 \times \pi \times r^2$. To study the influence of attachment time, the microcarrier-cell-suspension (MCS) was harvested at different time points after seeding. For both microcarrier types, the recovered area at adhesion times of 2, 4 and 24 h after seeding were analysed in a first step. As statistically significant differences were observed for both microcarrier types, adhesion times have been then divided in smaller sections: 3, 3.5, 4, 4.5, 5 and 24 h for soft microcarrier and 1, 2, 2.5, 3, 4 and 24 h for stiff microcarrier preparations.

2.5. Cryopreservation and thawing/warming procedures

Three cryo procedures were investigated in three biological (N) and technical (n) replicates each: (1) Slow freezing of suspended hiPSCs as gold standard. In this procedure, hiPSCs were detached with EDTA as described before (see section 2.1) and the cell number was determined using the Nucleo Counter NC-200 (ChemoMetec, Allerød, Denmark). $1\text{--}2 \times 10^6$ cells/ml were frozen using the automated computer-controlled freezer Ice-Cube 14S (SY-LAB, Neupurkersdorf, Austria) with a freezing rate of -1 °C per minute to -80 °C in 1 ml CryoStor CS10 medium (Stemcell Technologies, Vancouver, Canada) without any growth surface in standard 1.8 ml cryovials. Samples were stored below -140 °C and thawed after freezing in a 37 °C water bath until only a small ice crystal remained. Then, the cell suspension was transferred in a 15 ml centrifugation tube and 10 ml DMEM/F12 (Thermo Fisher Scientific, Waltham, USA) were added dropwise. The cells were subsequently centrifuged with $200 \times g$ for 3 min and resuspended in pre-warmed mTeSR™1 (37 °C) and seeded for recovery and further analysis in Matrigel-coated culture plates. (2) Slow freezing of hiPSCs on alginate microcarrier. In this procedure, $\sim 1.6 \times 10^6$ cells attached on microcarrier were frozen in 1 ml CryoStor CS10 in standard cryovials. Freezing and thawing procedures were performed as described for cryo procedure (1) above. For recovery and further analysis, the cells on microcarrier were transferred to ultra-low attachment culture plates (Corning, New York, USA) filled with pre-warmed mTeSR™1 culture medium supplemented with 3 μM ROCK-inhibitor. (3) Droplet-based vitrification. The microcarrier-cell-suspension (MCS) was vitrified by dripping 20 μl droplets directly into liquid nitrogen. For future standardised use of this method, e.g. in clinical translation, the use of liquid nitrogen sterilised with ultraviolet irradiation would be indicated [31].

A two-step protocol for the incubation of the MCS in cryo media as well as in warming media was applied based on the work using human embryonic stem cells of Richards et al. in 2004 [32]. In brief, 50 μl of the 4 °C pre-cooled vitrification solution 1 (VS1), consisting of 80% mTeSR™1, 10% ethylene glycol (EG; Sigma-Aldrich, St. Louis, USA) and 10% Me₂SO (Sigma-Aldrich, St. Louis, USA), was gently added to the pellet of 1 ml of the MCS ($\sim 1.6 \times 10^6$ cells), and incubated for 1 min without further resuspension. Due to sedimentation, centrifugation is not necessary. Next, 50 μl pre-cooled vitrification solution 2 (VS2) was added directly to the MCS in VS1, resuspended twice, and incubated for 5 s on the cells. VS2 consists of 20% EG, 20% Me₂SO, 0.4 M sucrose (Sigma-Aldrich, St. Louis, USA) diluted in mTeSR™1, and 30% mTeSR™1 culture medium. Subsequently, the cell-VS1-VS2-suspension was dropped quickly in 20 μl droplets into liquid nitrogen bath with separated compartments to prevent agglomeration. Successful vitrification was assessed by the transparency of the droplets. In addition, DSC data of the VS2 medium proved a virtually ice-free vitrification at the instruments ballistic cooling rate, which is 2100 °C/min maximum for the applied Perkin Elmer DSC8500. Even the average cooling rates in our experimental setup are higher. The DSC curves at a heating rate of +10 °C/min exhibit a glass transition at -129 °C and a devitrification onset at -104 °C [33]. The Arrhenian parameters for VS medium devitrification kinetics were determined to $E_A = 54.3 \pm 2.4$ kJ/mol and $\ln(K_0 \cdot \text{min}) = 38.4 \pm 1.8$. The rewarming procedure was performed with warming solution 1 and 2 (WS1 and WS2), consisting of 0.2 M and 0.1 M sucrose solution in mTeSR™1, respectively. Both, WS1 and WS2 were supplemented with 3 μM ROCK-inhibitor Y-27632 and prewarmed to 37 °C. For warming, vitrified droplets were incubated for 1 min in WS1, supernatant was aspirated carefully and WS2 was added for 5 min. WS2 was exchanged with prewarmed mTeSR™1 culture medium supplemented with 3 μM ROCK-inhibitor. The adherent cells on microcarriers were transferred into ultra-low attachment culture plates for recovery and quality control.

2.6. Scanning electron microscopy (SEM)

To exclude ‘background noises’ (too many apoptotic bodies in SEM analysis) resulting from apoptotic events upon warming after vitrification, samples were fixed after a recovery phase of 24 h [34]. Therefore, the samples of three biological replicates were pooled, washed in PBS without Ca²⁺ and Mg²⁺ and fixed in glutaraldehyde (Sigma-Aldrich, St. Louis, USA) supplemented in sodium cacodylate buffer (Sigma-Aldrich, St. Louis, USA) at 4 °C overnight. For treatment procedure, the microcarriers were placed in cell culture inserts (PIXP01250, Merck Millipore, Darmstadt, Germany) and the preparation was performed as described previously [35,36]. Briefly, the samples were washed in sodium cacodylate buffer, post-fixed in 2% osmium tetroxide (Roth, Karlsruhe, Germany) and in 1% tannic acid (Sigma-Aldrich, St. Louis, USA). The

samples were dehydrated in increasing ethanol series, and dried in hexamethyldisilazane (HMDS, Sigma-Aldrich, St. Louis, USA) as described elsewhere [37]. Finally, the samples were coated with carbon (Sigma-Aldrich, St. Louis, USA), and studied in field emission scanning electron microscope Phillips FESEM XL30 (FEI, Eindhoven, Netherlands) with 5 kV in secondary electron (SE)-mode and 10 mm working distance.

2.7. Staining of actin filaments and determination of viability and recovered area

The actin cytoskeleton plays a major role in motility, mechano-transduction, adhesion, and signal-response coupling, e.g. for apoptosis [38], which is why we investigated its alteration regarding adhesion time and matrix elasticity. On both microcarrier types, F-actin staining was analysed after 1 h, 24 h, and the optimal adhesion time, respectively. For F-actin staining, hiPSCs on both microcarrier types were fixed for 20 min in fixation buffer (BD Bioscience, Franklin Lakes, USA) at room temperature and were subsequently permeabilised with 0.2% Triton-X-100 (Sigma Aldrich, St. Louis, USA) for 20 min at room temperature. To avoid unspecific staining, samples were blocked for 30 min using 0.2% Tween (Sigma Aldrich, St. Louis, USA) and 1% BSA (Thermo Fisher Scientific, Waltham, USA). F-actin was stained with BODIPY® FL phalloidin (Thermo Fisher Scientific, Waltham, USA) and cell's nuclei with NucBlue™ Live Cell Stain Ready Probes™ reagent (Thermo Fisher Scientific, Waltham, USA) according to manufacturer's instructions. Images were taken with the confocal laser scanning microscope TCS SP8 (CLSM; Leica, Wetzlar, Germany). The viability of adherent cells on microcarrier was determined via image analysis using ImageJ (NIH, Bethesda, USA) after a staining with 20 µg/ml fluorescein diacetate (FDA, green fluorescent signal in metabolic active, viable cells) and 10 µg/ml ethidium bromide (EB, red fluorescent signal in porous, dead cells) (both Invitrogen, Karlsruhe, Germany) in DMEM/F12. Fluorescence images were taken using a TE 300 Nikon microscope, areas of interest (hiPSC colonies on microcarrier) were selected, and the intensities from both channels were put in relation to calculate the viability of the 3D, multicellular samples as described previously [39]. The area overgrown with hiPSCs was determined by the area detection using NIS-Elements 4.6 of FDA-stained cells. In three biological replicates, eight technical replicates each were evaluated.

2.8. Quantitative reverse transcriptase polymerase chain reaction

Potential alterations in gene expression level were analysed by quantitative polymerase chain reaction using the QuantStudio™7 Flex Real-Time PCR System (Thermo Fisher Scientific, Waltham, USA) in three biological and two technical replicates. In order to see a substantial effect on gene expression upon warming, cells were fixed after a recovery phase of 5 days. Therefore, RNA was extracted with the RNeasy Micro Kit 50 (Qiagen, Venlo, Netherlands) according to manufacturer's advice. Subsequently 250 ng RNA was amplified using a SimpliAmp Thermal Cycler (Thermo Fisher Scientific, Waltham, USA) in combination with the High-Capacity cDNA Reverse Transcription Kit (Thermo Fisher Scientific, Waltham, USA) to cDNA according to manufacturer's advice. Quantification of gene expression relies on real time fluorescence measurements with TaqMan™ probe (Thermo Fisher Scientific, Waltham, USA) and proportional increase of fluorescence signal to amount of amplified product. Stemness markers (TERT, SOX2, POU5F1 and NANOG) have been assessed. For relative quantification, the $2^{-\Delta\Delta Ct}$ method was applied and HPRT1 and GAPDH served as endogenous reference.

2.9. Flow cytometry

Alteration in stemness characteristics after cryopreservation was assessed by flow cytometric analysis using the FACS Aria™ III (BD

Biosciences, Franklin Lakes, USA). Therefore, cells were fixed, also after a recovery time of 5 days, permeabilised and stained with the extracellular marker TRA-1-81 (FITC) and intracellular marker POU5F1 (PE) as well as NANOG (PE) (all BD Biosciences, Franklin Lakes, USA) according to manufacturer's advice. Fixation and permeabilization buffer (both BD Biosciences, Franklin Lakes, USA) were used according to manufacturer's advice. Samples were stained in FACS-buffer consisting of phosphate buffered saline supplemented with 2% fetal bovine serum (Thermo Fisher Scientific, Waltham, USA) and 0.5 g sodium acid (Sigma-Aldrich, St. Louis, USA). Per approach, 1×10^6 cells were prepared in three biological replicates and at least 1×10^4 events were detected.

2.10. Statistical evaluation

Graphical illustration of data and statistical analyses were performed using OriginPro 2016. Differences between groups were tested with a one-way-ANOVA with Tukey post-hoc test and $p < 0.05$ were considered significant in three biological replicates N (technical replicates n differed among the applied readout methods).

3. Results

3.1. Recovery of iPSCs after adherent vitrification

To quantify the recovery of vitrified adherent hiPSC after warming, the area covered by hiPSCs was determined via image analysis immediately before cryopreservation and 24 h after warming to exclude cryo-induced apoptotic effects. Fig. 1 shows the percentage of the recovered area for adherent hiPSCs on soft (Fig. 1 A) and stiff (Fig. 1 B) alginate microcarriers after vitrification. The data has been normalised to the non-frozen control. The resolution for the adhesion time intervals before cryopreservation was pre-determined in pilot screening studies and was increased in the present study around the found optimum of t_a (opt.) = 4 h for the soft microcarrier type and t_a (opt.) = 2.5 h for stiff carrier. For hiPSCs on soft microcarriers, adhesion times t_a of 3, 3.5, 4, 4.5, 5, and 24 h were investigated and for hiPSCs on stiff microcarrier, adhesion times t_a of 1, 2, 2.5, 3, 4, and 24 h. With a maximum recovered area of $42 \pm 9\%$, hiPSCs on soft microcarrier after t_a (opt, soft) = 4 h showed the best result (Fig. 1 A). The maximum recovered area for hiPSCs on stiff microcarriers however was detected in the sample with $t_a = 3$ h. The increased time resolution of the present experiments indicated that the actual t_a (opt.) for stiff microcarriers is 3 h instead of the previously assumed 2.5 h resulting from the pilot study and was adjusted in the further study. The recovered area for t_a (opt, stiff) = 3 h is 35% with a relatively high standard deviation of $\pm 18\%$ (Fig. 1 B). For both microcarrier types, a deviation in both directions from the optimal adhesion time prior to vitrification leads to a decreased cell recovery. Representative microscopic images are shown for the soft microcarriers in Fig. 2. The cellular viability of vitrified hiPSCs was determined 24 h after warming to exclude cryo-induced apoptotic events using an ethidium bromide and fluorescein diacetate staining and viability is indicated by the corresponding % values in the fluorescence images. With a viability of 90%, samples vitrified after t_a (opt, soft) showed the best cell recovery. As a cryo-control, the microcarrier cell suspension was frozen by applying a conventional slow freezing protocol in standard cryo vials, but no attached cells could be recovered. Immediately after thawing (0 h) 100% of the cells were detached from the microcarrier (Suppl. Figure 2) and no re-attachment could be observed afterwards.

3.2. Influence of surface stiffness on hiPSCs

Two different stiffness grades of alginate microcarriers as growth surfaces with variable elasticity for hiPSCs were examined. Stiffness was characterised by the storage (G') and loss (G'') moduli. At that, the storage modulus describes the elastic, reversible behaviour as the

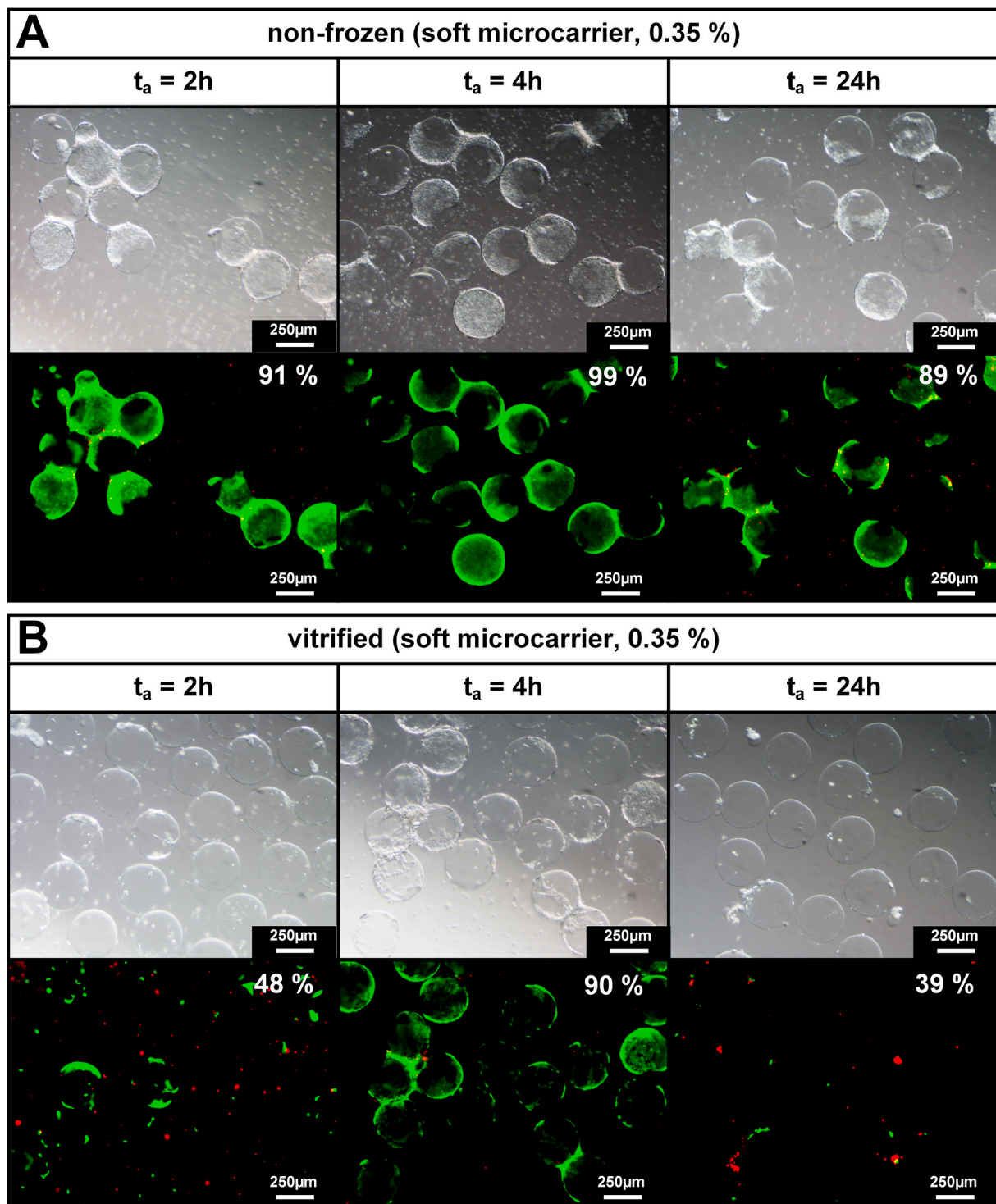


Fig. 2. Representative images of non-frozen and vitrified hiPSCs on soft alginate microcarrier. Fluorescence and transmitted-light images of hiPSCs on soft (0.35 %) alginate microcarrier. Images were taken 2, 4, and 24 h after seeding (t_a = adhesion time). After vitrification, $t_a = 4$ h showed highest cell preservation. Viability has been counted via image analysis and is given as percentage in each fluorescent image (biological replicates $N = 3$, technical replicates $n = 3$). Contrast has been enhanced for better visibility and scale bars are 250 μm .

available portion of introduced energy following a deformation. In contrast, lost energy presents the irreversible, viscous characteristic of a material parameterised by the loss modulus. Solutions with $G'' > G'$ show a dominant viscous behaviour. The reverse is the case in gels and the viscoelastic properties shift to $G' > G''$ [40]. The storage and loss

moduli of 0.35% and 0.65% alginate solutions and gels were determined via dynamic mechanical analyses (Suppl. Figure 1). With increasing alginate concentration more viscous solutions were obtained. Moreover, 0.65% alginate samples exhibited a more cross-linked and stiffer network after gelation than 0.35% alginates. In addition, compression

studies monitoring the elastic modulus of the gelled matrices revealed increased and more reproducible gel stiffnesses at higher alginate concentrations (0.35%: 39 ± 9 kPa; 0.65%: 44 ± 6 kPa, statistically significant different, $p < 0.05$) (Suppl. Figure 1C). The morphology of the hiPSCs was examined after different adhesion times on both microcarrier types via SEM and immunocytochemistry staining of F-actin (Fig. 3). After a short adhesion time of $t_a = 1$ h after seeding, no distinct F-actin fibres were visible, the accordant signals were located adjacent to the cell's nuclei. SEM study revealed that the cell-matrix contact as well as cell-cell contacts were tight, however some individual cells and small spherical objects, most likely apoptotic bodies, of 0.5–2 μm in diameter, were observed on both microcarrier types (red asterisks, Fig. 3). After applying the found optima for the adhesion time on both microcarrier types ($t_{a(\text{opt, stiff})} = 3$ h, $t_{a(\text{opt, soft})} = 4$ h), several spherical cells with or without microvilli indicate an ongoing apoptosis (red asterisks, Fig. 3A and B) but the cells already spread around the microcarrier and the amount of F-actin fibres increased. Cells at $t_a = 24$ h showed close cell-cell contacts and apoptotic bodies were absent. The immunocytochemistry staining showed distinct F-actin filaments with which the cells spread towards neighbouring cells and the microcarrier surface, indicating a stretched, flat, and elongated cell shape minimizing their flexibility.

3.3. Effect of vitrification on surface morphology of hiPSCs

The surface morphology of adherent hiPSCs on soft (Fig. 4) and stiff (Fig. 5) microcarriers were examined via SEM in the non-frozen control and immediately upon warming after droplet-based vitrification. In detail, two adhesion time points for each microcarrier type were examined: $t_{a(\text{opt.})}$ as well as $t_a = 24$ h. Both non-frozen controls at $t_{a(\text{opt.})}$ showed few apoptotic bodies and a highly similar morphology of the adherent hiPSCs. Also, the surface morphology of the non-frozen cells in direct comparison with the morphology of adherent hiPSCs immediately upon warming did not reveal any differences. The non-frozen controls at $t_a = 24$ h for both microcarrier types exhibit widely overgrown surface and spread hiPSCs with and without microvilli. Here too, no differences in morphology between the hiPSCs on soft and stiff microcarrier were visible. However, after droplet-based vitrification with $t_a = 24$ h, hiPSCs on stiff microcarrier showed holes, most likely ruptures, in cell membranes and gaps between cells (red dashed ovals in Fig. 5 at $t_a = 24$ h). Few similar alterations in morphology could be seen in the non-frozen controls as well as on the soft microcarrier at $t_a = 24$ h after vitrification but SEM images showed a significant increase in number of ruptures on the stiff microcarrier. A change in the ultrastructure of the alginate growth surface was documented as well. Whereas the alginate reveals a highly regular structure before cryopreservation, especially in Fig. 4 at $t_a = 4$ h an alteration of the structure to an inhomogeneous and fuzzy appearance was detected after vitrification.

3.4. Influence of adherent vitrification on protein and gene expression level

Stem-cell specific characteristics after droplet-based vitrification at optimal adhesion time $t_{a(\text{opt.})}$ and analysed growth surface (soft) conditions were assessed at the protein level via FACS and the genetic level via qPCR 5 days after warming. For FACS analysis the stemness markers NANOG, POU5F1, and TRA-1-81 were examined (Fig. 6 A). Vitrified hiPSCs on both microcarrier types (t_a (soft) = 4 h) were compared against the non-frozen control as well as against the slow frozen cryo control after a recovery time of five days. Results are displayed in Fig. 6 A (non-frozen control ($84 \pm 3\%$), slow frozen cryo control $71 \pm 7\%$, vitrified sample $84 \pm 5\%$). The bars representing the cryo control indicate a slight reduction of the stemness characteristics. However, the differences are not statistically significant ($p < 0.05$). The FACS analysis was supported by a qPCR analysis using the markers TERT to show iPSC-

characteristic telomerase activity, and SOX2, NANOG, POU5F1 for markers of stemness. The housekeeping genes HPRT1 and GAPDH served as endogenous controls and reference genes for normalization (= ΔC_t ; calibrator) were generated by C_t mean of non-frozen control samples on soft and stiff microcarrier, respectively. Results are shown as fold change in Fig. 6 B. Highest increase in fold change is the upregulation of the SOX2 and highest decrease in fold exchange has been detected for TERT. However even these outlier results are within the range 0.5–2 of logarithmic fold exchange that is assumed as no significant change of the examined population.

4. Discussion

4.1. Droplet-based vitrification enables application-oriented adherent cryopreservation

Here the droplet-based vitrification process has been compared to the standard conventional slow freezing of adherent cells on the same alginate microcarrier types. It was visually verified that the samples had reached cryogenic temperatures without crystallization and a vitrification was actually achieved (transparency of the sample droplets). Whereas no cells were recovered after slow freezing (Suppl. Figure 2), adherent hiPSC on microcarrier could be preserved by vitrification (Fig. 1). The success of cell recovery after vitrification was shown to be dependent on the adhesion time of the hiPSCs before vitrification as well as on the elastic properties of the growth surface. Such an optimization of adhesion time prior to cryopreservation had been shown for slow freezing of mesenchymal stem cells (MSCs) on three dimensional alginate-gelatine sponges before [36]. Here, the found t_a optimum, resulting in highest recovered cell number and viability, was 2 h. In the present study, optimal adhesion times of hiPSCs were analysed in correlation with matrix elasticity of two alginate microcarrier types, whereby best cell recovery of more than 40% could be observed on soft microcarriers after an adhesion time of t_a (opt. soft) = 4 h (Fig. 1). For stiff carriers, the slightest cell loss was documented after 3 h, with a recovered area of 38%. Viability staining using FDA to show metabolic active cells and ethidium bromide to stain dead cell nuclei supported the finding of microcarrier-specific optima of the adhesion time and the superiority of the soft growth surface (Fig. 2). However, viability via metabolic activity can only be one partial parameter to determine the effectiveness of a cryopreservation routine as has it has already been shown in other studies [41,42]. In direct comparison with conventional freezing of hiPSCs as single cells or cell clumps in suspension [43], the droplet-based vitrification shown here immediately provides ready-to-use adherent hiPSCs on a growth surface upon warming.

4.2. SEM analysis reveals apoptotic events during inoculation

To investigate cellular characteristics at the adhesion time optima t_a (opt.) determined in this study for the subsequent vitrification, comparative SEM analysis and immunocytochemistry staining for the cytoskeleton protein actin were performed on both microcarrier types (Fig. 3). The SEM analysis reveals the surface morphology of cells and showed few cells without microvilli (<5%), which agrees with previous ultrastructural description of hiPSCs [44]. After short adhesion times for both microcarrier types, membrane blebbing immediately after seeding was detected as an indicator of the onset of apoptosis [35]. Since stem cells are well-known to show dissociation-induced apoptosis [45], it is highly likely that this so-called anoikis had been documented here in accordance with Zhang et al. 2018 [46]. At $t_a = 24$ h this blebbing could no longer be observed, indicating that the programmed cell death mechanisms were completed and that the affected cells were disintegrated. Addition of ROCK inhibitor had already been shown to be highly effective to reduce anoikis upon dissociation [19] as well as upon cryopreservation [47] and is usually added at a concentration of 10 μM upon thawing in the cultivation media. In order to minimise but not

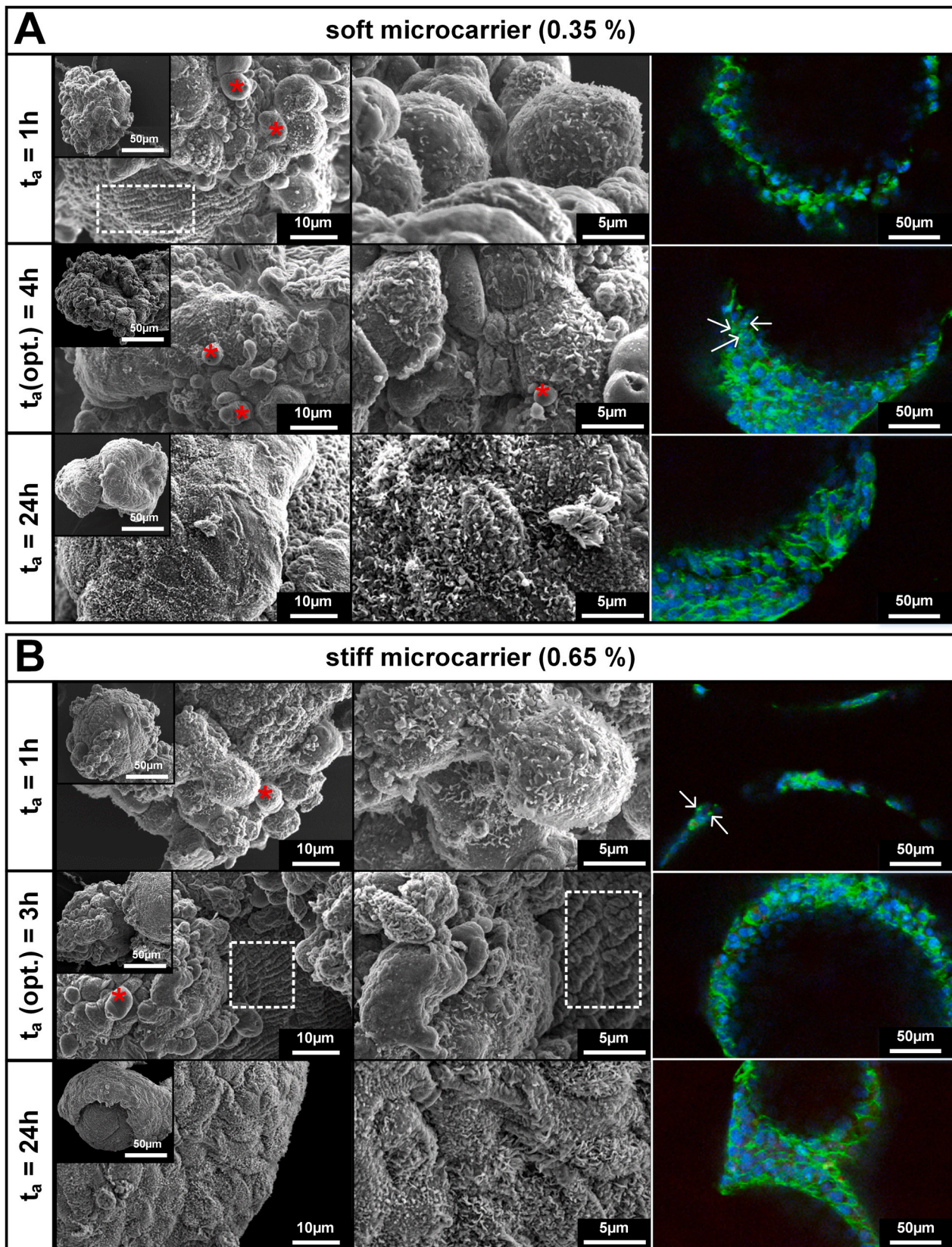


Fig. 3. Influence of different adhesion times on morphology and F-actin development of hiPSCs cultured on soft and stiff alginate microcarrier. Representative SEM and fluorescence images of adherent hiPSCs on soft (A) and stiff (B) alginate microcarrier at different time points after seeding (adhesion times $t_a = 1$ h, 3 h, and 24 h). Red asterisks indicate apoptotic bodies. White dashed rectangles indicated alginate carrier surface without hiPSCs. Right column shows confocal laser scanning images after antibody staining of F-actin (green) and nuclei (blue) of hiPSCs on alginate microcarrier. White arrows indicate fragmented nuclei (sign of apoptosis) ($n = 3$). (For interpretation of the references to colour in this figure legend, the reader is referred to the Web version of this article.)

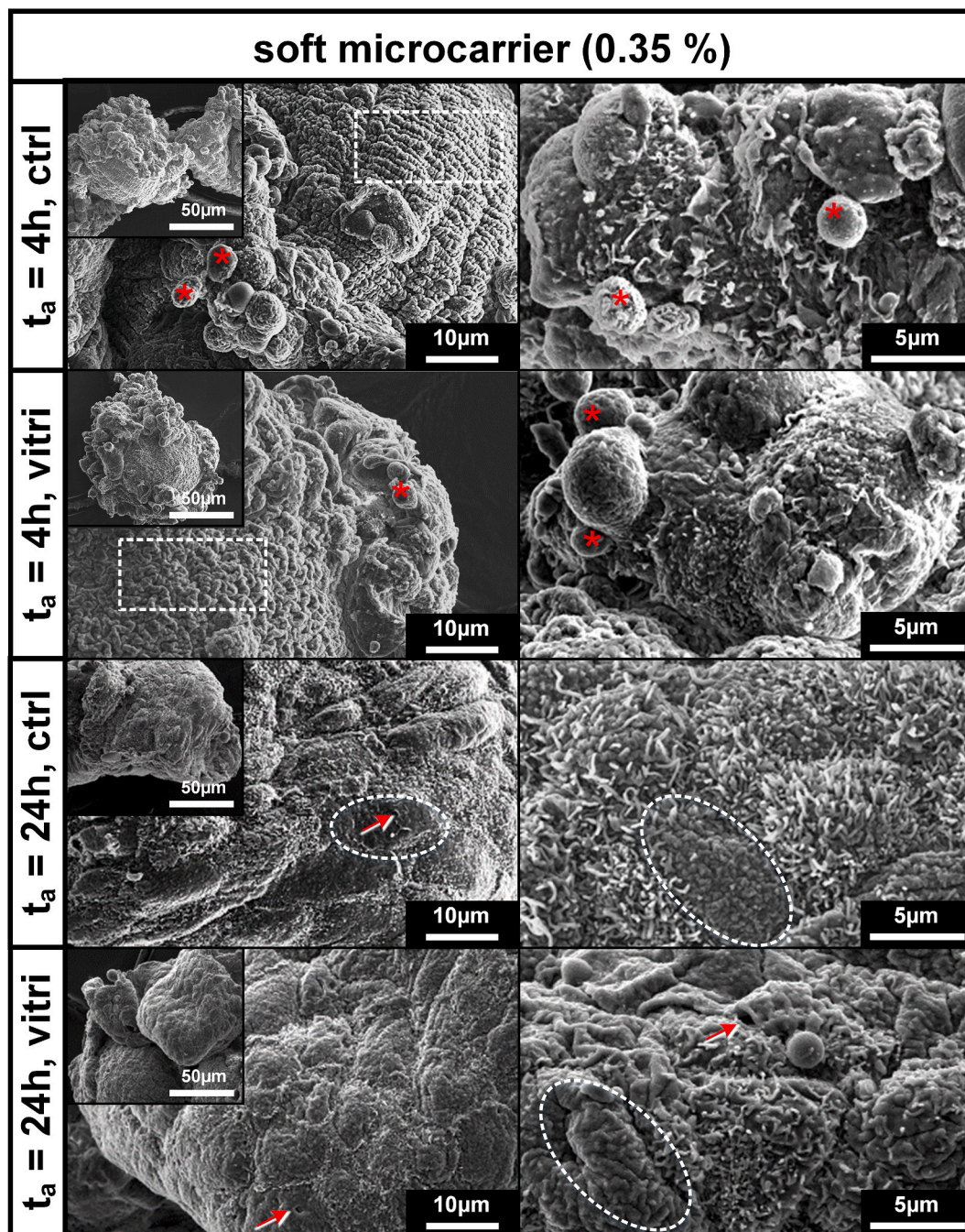


Fig. 4. Surface morphology of non-frozen and vitrified hiPSCs on soft alginate microcarrier immediately after warming. Representative SEM images show hiPSCs after the optimum adhesion time ($t_{a(opt., soft)} = 4 h$) and after 24 h for the unfrozen control (ctrl) as well as for the vitrified hiPSCs (vitri) immediately after warming. White dashed rectangles show pure alginate surfaces without cells, red asterisks show apoptotic bodies. White dashed ovals indicate cells without microvilli. Red arrows in samples after $t_a = 24 h$ show ruptures in cell membranes. (For interpretation of the references to colour in this figure legend, the reader is referred to the Web version of this article.)

eliminate anoikis, a reduced concentration of 3 μM ROCK was added to the media for 24 h upon thawing/warming. SEM images as well as immunocytochemistry staining of actin filaments indicate that the cells exhibit highly similar morphology at the two detected optima in adhesion time prior to a successful vitrification for the two microcarrier types. Representative images in Fig. 3 show that hiPSCs at both $t_{a(opt.)}$ closed intercellular gaps and that the F-actin signal increased. Now, single cells within the colonies can be distinguished by the formed distinct F-actin network around the NucBlue™-stained nuclei showing an intact cytoskeleton.

4.3. Structural change of alginate after vitrification process

SEM analysis shown in Figs. 4 and 5 revealed changes in alginate surface after vitrification (highlighted in dashed rectangles). Whereas the alginate microstructures in the non-frozen control exhibit a highly regular structure, the alginate after vitrification appears messy. In order to be able to discuss this discovery more precisely, however, further experiments on the pure microcarrier material without cell growth are necessary, which were not part of this work. Here we can only speculate that the cryopreservation media, devitrification, or cell attachment were the cause of these alterations.

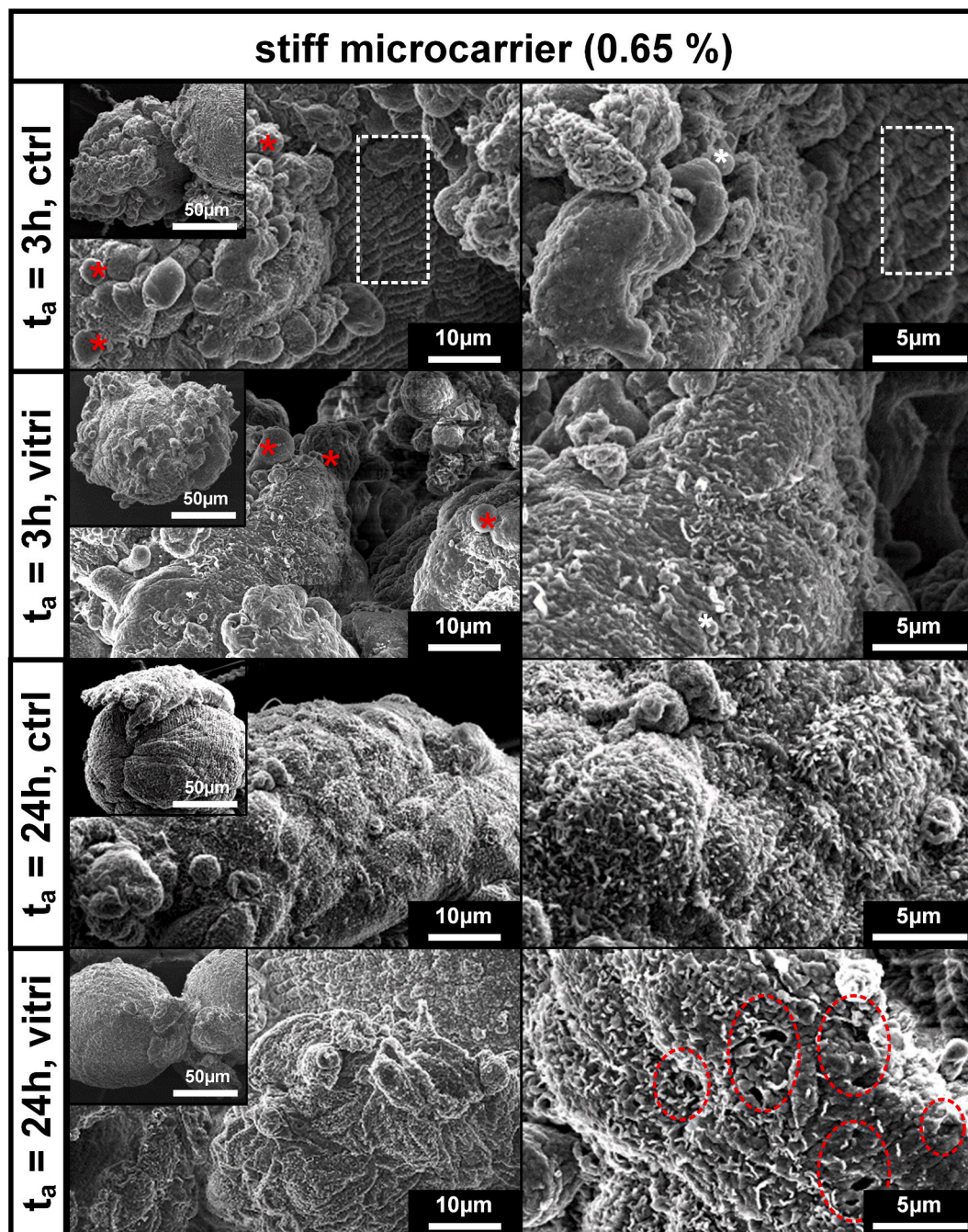


Fig. 5. Surface morphology of hiPSCs on stiff alginate microcarrier in non-frozen control and after vitrification immediately after warming. Representative SEM images show hiPSCs after the optimum adhesion time ($t_{a(\text{opt.}, \text{stiff})} = 3 \text{ h}$) and after 24 h for the non-frozen control (ctrl) as well as for the vitrified hiPSCs (vitri) immediately after warming. White dashed rectangles show pure alginate surfaces without cells, red asterisks show apoptotic bodies. Red dashed ovals in samples after 24 h adhesion time show ruptures in cell membranes, significantly increased after vitrification. (For interpretation of the references to colour in this figure legend, the reader is referred to the Web version of this article.)

4.4. Accumulation of membrane ruptures and intercellular gaps after vitrification on stiff microcarrier

Surface structure of adherent cells had been investigated after droplet-based vitrification in direct comparison with a non-frozen control at $t_{a(\text{opt.})}$ and $t_a = 24 \text{ h}$ (Fig. 4: soft microcarrier, Fig. 5: stiff microcarrier). Cell morphology before and after vitrification on both microcarrier types appeared very similar. hiPSC of $t_a = 24 \text{ h}$ on soft carriers showed only few intercellular gaps and membrane ruptures, prior as well as post vitrification. In contrast, identically cultured hiPSCs on stiff carriers exhibited significant numbers of such injuries after

vitrification (red dashed ovals, Fig. 5). Previous studies have already shown a correlation between the stiffness of the surface and the stiffness of the cytoskeleton [48]. Therefore, we hypothesize based on our findings, that the hiPSC cytoskeleton on stiff microcarriers is less mechanically flexible due to the support of the surrounding matrix and thus more prone to damaging mechanical effects during the applied cryopreservation routine. First, drastic increased osmotic pressure due to media change occurs: during incubation in cryo media with impermeable CPAs (0.3 M trehalose) of relatively high osmolarity compared to the cultivation medium, microcarrier and cells dehydrate before cooling. Addition of reduced osmolarity warming media reverses this process and

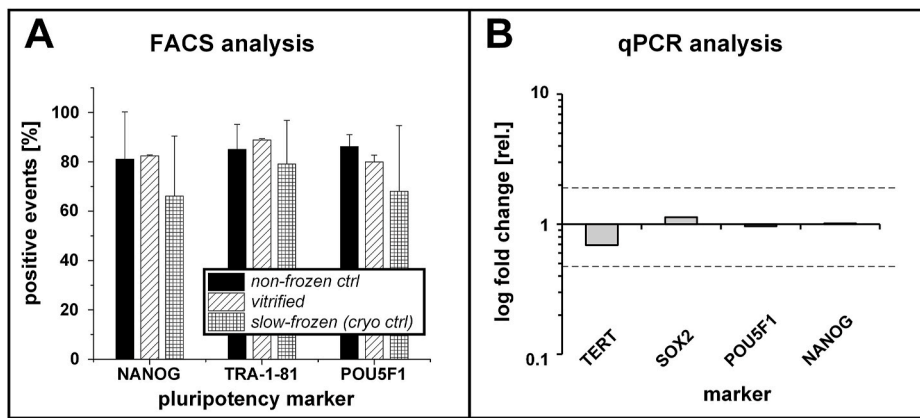


Fig. 6. Protein and gene expression levels after adherent droplet-based vitrification of hiPSCs on soft alginate microcarrier.

(A) Percentage of positive FACS events for stemness antibodies NANOG, TRA-1-81 and POU5F1 in non-frozen control, adherently vitrified on soft microcarrier and slow frozen hiPSCs in suspension without microcarrier (cryo ctrl). No statistically significant difference was detected ($N = 3$, $n = 1$). (B) Fold change of the gene expression for stemness markers TERT, SOX2, POU5F1, and NANOG of the vitrified samples are shown. Fold change lies in the range 0.5–2 and is therefore assumed as not significantly different compared to the non-frozen hiPSCs, which served as reference ($N = 3$, $n = 2$).

causes swelling of the alginate microcarrier as well as heavy cell volume regulation. Secondly, devitrification cannot be excluded: the achieved cooling rates by dripping of the sample droplets in liquid nitrogen in concert with the added CPAs enabled an ice-free vitrification of the sample during cooling. To determine the cooling rate, the time between the first contact of the droplet with liquid nitrogen and the termination of boiling was measured. Together with the sample temperature of 4 °C at the beginning to the end temperature of liquid nitrogen of –196.7 °C, cooling rates were found to be between 6000 and 9000 °C/min). However, the warming rates realised by dripping the transparent, vitrified samples in 37 °C warming solution resulted in opaque droplets indicating ice formation. Even though our recent DSC studies on the applied vitrification solution showed its stability (see section 3.5), the final sample here (mixture of vitrification and hiPSC microcarrier solution), could lead to devitrification and would fall under the term “rapid cooling”, defined in Ref. [49]. The devitrification process results in crystallization with again high hydraulic pressure for the biological sample. Both damaging effects have already been extensively studied, especially in conventional slow freezing routines for mammalian cells [50,51]. In future studies, warming could be optimised, for example by inductive heating of nanoparticles to prevent devitrification, as has been shown for porcine arterial and heart valve tissues [52] and hiPSCs [53].

4.5. Adhesion time and matrix elasticity hypothesis

That cell stiffness depends on the stiffness of growth surface has already been reported [48]. It is also known, that the substrate stiffness influences differentiation processes and cell fate [54,25]. Additionally, scaffold-based cryopreservation approaches of stem cells on or in microcarriers [24,55] or sponge-like growth structures are subjects of research [36,56]. Findings in the present study showed that the membrane elasticity of cells, determined by the adhesion time as well as the characteristics of their growth surface, have an influence on their recovery after adherent cryopreservation (Fig. 7). Our data strongly suggests that there is an optimal adhesion time prior to cryopreservation in accordance with [36] and shows that this optimum depends on matrix elasticity and lead to the hypothesis that two basic damaging mechanisms determine the success of an adherent cryopreservation routine. Even though these mechanisms most likely act in concert, each of them is predominant in the sub- and supra-optimal phase, respectively. The predominant damaging mechanism after adhesion time had been indicated via SEM analysis (Figs. 4 and 5). After the dissociation of the adherent cells necessary for inoculation, cells are in suspension and spherical. In this cell state, the proportion of filamentous actin is lower due to the depolymerisation to globular actin. Hence, the cells are more mechanically flexible with fewer and shorter actin filaments. Cells in this state are ready to form integrin-mediated focal contacts, which are anchored in actin fibres as soon as a growth surface is provided [57].

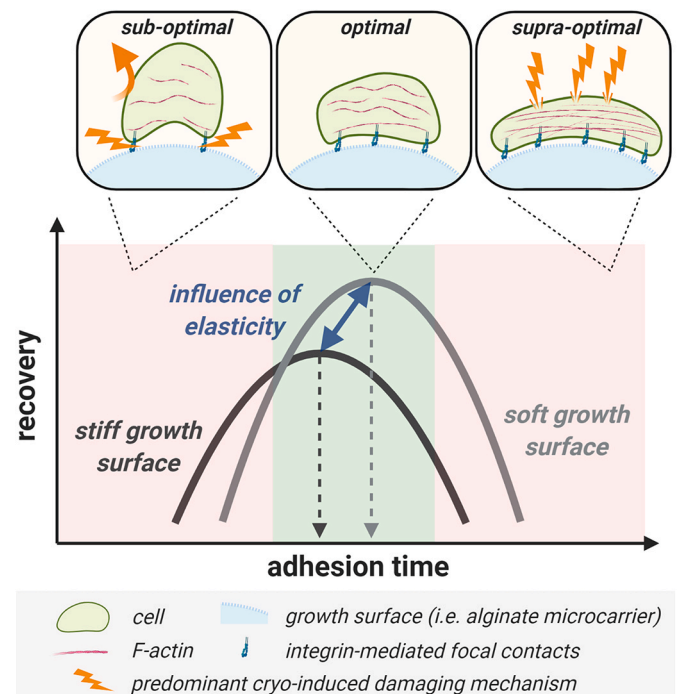


Fig. 7. Adhesion time and matrix elasticity hypothesis.

Recovery of adherent cells after cryopreservation correlates with the cytoskeletal state of the cells depending on adhesion time as well as on the matrix and thus growth surface elasticity. The predominantly damaging event in the sub-optimal range is the detachment of cells. In the supra-optimal range it is the inability of increasingly inelastic cytoskeletal structures to tolerate ice formation (created with biorender.com).

This implies that after a short adhesion time, i.e. in the sub-optimal range, there is only a small number of focal contacts present that attach the cells on the surface. Due to the mechanical stress during cryopreservation (liquid flows during media change, incipient ice crystal formation during thawing), some contacts do not withstand the pressure, so the cell loses its connection and is detached from the surface. A reduction in recovered cell number after a short incubation time corresponds to the findings in Ref. [36]. With a pronounced cytoskeleton indicated by distinct F-actin networks (Fig. 3, $t_a = 24$ h), cells are less flexible [58] and thus enter a supra-optimal phase regarding the recovery post cryopreservation. On the analysed stiff growth surface, a multitude of membrane ruptures as well as intercellular gaps could be detected (Fig. 5, red dashed ovals). Due to increased adhesion times in concert with stiff growth surfaces, cytoskeletal structures are less elastic

and thus more sensible to forming ice crystals during warming and appearing heavy water influx upon thawing. Even though the actin polymerization is very fast (e.g. 7 nm s^{-1} for fibroblasts [59]) as its crucial for nearly any cellular process [58], the process is not fast enough to prevent damages especially during the cryo-relevant volume regulation or ice formation that occurs within milliseconds to seconds [60,61]. Like an optimal cooling rate in conventional slow freezing processes [62], the here claimed adhesion time optimum is highly likely to be cell-type specific as size, hydraulic conductivity and osmotic active volumes differ among cell types. Whereas $t_a(\text{opt.})$ for hiPSCs is in the range of 3 and 4 h depending on the matrix elasticity, 2 h was determined as $t_a(\text{opt.})$ for MSCs [36]. In this previous study, MSCs were seeded on three dimensional alginate-gelatin cryogel scaffolds and incubated for 0.5, 2, and 24 h. After 2 h cultivation time, the most successful results regarding cell number, motility, cell contacts and membrane integrity were achieved. Our optimal adhesion time for vitrification and highest preservation of cell areas on soft microcarrier was at $t_a = 4 \text{ h}$ with 41.7% (± 4.2) receipt and on stiff carrier at 3 h with retention of 34.7% (± 18.4) and could most likely be further optimised by adjusting the concentration of the apoptosis-inhibitor ROCK to 10 μM . Considering that the cytoskeleton plays a major role in cell's adhesion, stiffness, volume regulation etc., and that its structure is highly conserved in eukaryotes [63], the introduced hypothesis is most likely generic for adherent cell types.

4.6. Vitrification causes no alteration on analysed protein and gene expression level after warming

The FACS results while showing a slight decrease in the cryo control, did not exhibit statistically significant difference in stemness marker levels when comparing cryopreserved samples to non-frozen controls. The stemness characteristics, validated by three prominent markers NANOG, TRA-1-81, and POU5F1, of the hiPSCs could be maintained. Likewise, the gene expression analysed via qPCR did not show statistically significant differences compared to the non-frozen control. The stemness markers NANOG, TRA-1-81, and POU5F1 were taken into consideration in this analysis again as well as TERT as indicator for the telomerase activity in stem cells. As no cells could be recovered after slow freezing of adherent hiPSCs on alginate microcarrier neither FACS nor qPCR could be performed to reveal potential differences between both cryopreservation methods. Therefore conventional slow cooling with enzymatic dissociated hiPSCs in suspension served as a cryo control in our FACS analysis.

4.7. Droplet-based vitrification produce application-oriented, ready-to-use products

In the context of cell-based assays in pharmacological screenings or in suspension-based large scale cell productions for therapeutic approaches, there is an increasing demand in storable but ready-to-use products. While cryopreservation is still the only possibility to stably store viable biological material for extended periods of time, state-of-the-art cryotechnological infrastructure has been designed for slow freezing of single cells in suspension. As medically relevant human cell systems like hiPSCs and hiPSC derived specialised cell types are anchorage dependent, the necessary processes of cell detachment and dissociation disable application-oriented storage protocols but require time-intensive re-cultivation and re-differentiation steps. Consumables like cryovials, freezing devices and cryogenic storage tanks in biobanking facilities are limited to the conventional slow freezing cryopreservation regime and current vitrification techniques are usually cumbersome, require skilled handling and are not ready for high throughput. It is welcomed that recent studies cope with cryopreservation of adherent cells with a focus on slow freezing approaches [20,64, 65] as well as scaffold-free vitrification approaches of human myoblast cell sheets [66], even though currently in small scale. In this study, we

developed a vitrification-based method for adherent hiPSCs cultured and cryopreserved on alginate microcarriers as a ready-to-use product for inoculation of suspension-based bioreactors upon warming. A comparative study of two different microcarrier types revealed the influence of adhesion time and matrix elasticity on the cryopreservation success. The droplet-based procedure can in future applications be adapted using microfluidic systems as has been shown for cryopreservation of suspended hepatocytes [67] to increase the throughput and thus be able to feed the raising demands on ready-to-use stocks for inoculation of e.g. suspension-based bioreactors.

Declaration of competing interest

There are no potential conflicts of interest.

Acknowledgements

This study was funded under the Seventh Framework Programme (FP7) of the European Commission (FP7-HEALTH), grant agreement: 601865 (DropTech). We thank Dr. Rachel Steeg for careful proofreading.

Appendix A. Supplementary data

Supplementary data to this article can be found online at <https://doi.org/10.1016/j.cryobiol.2021.09.010>.

References

- [1] H. Inoue, N. Nagata, H. Kurokawa, S. Yamanaka, iPS cells: a game changer for future medicine, *EMBO J.* 33 (2014) 409–417, <https://doi.org/10.1002/embj.201387098>.
- [2] K. Takahashi, S. Yamanaka, Induction of pluripotent stem cells from mouse embryonic and adult fibroblast cultures by defined factors, *Cell* 126 (2006) 663–676, <https://doi.org/10.1016/j.cell.2006.07.024>.
- [3] P. Karagiannis, K. Takahashi, M. Saito, Y. Yoshida, K. Okita, A. Watanabe, H. Inoue, J.K. Yamashita, M. Todani, M. Nakagawa, M. Osawa, Y. Yashiro, S. Yamanaka, K. Osafune, Induced pluripotent stem cells and their use in human models of disease and development, *Physiol. Rev.* 99 (2019) 79–114, <https://doi.org/10.1152/physrev.00039.2017>.
- [4] S. Sances, L.I. Bruijn, S. Chandran, K. Eggan, R. Ho, J.R. Klim, M.R. Livesey, E. Lowry, J.D. Macklis, D. Rushton, C. Sadegh, D. Sareen, H. Wichterle, S.-C. Zhang, C.N. Svendsen, Modeling ALS with motor neurons derived from human induced pluripotent stem cells, *Nat. Neurosci.* 19 (2016) 542–553, <https://doi.org/10.1038/nn.4273>.
- [5] A. Artero Castro, D. Lukovic, P. Jendelova, S. Erceg, Concise review: human induced pluripotent stem cell models of retinitis pigmentosa, *Stem Cell.* 36 (2018) 474–481, <https://doi.org/10.1002/stem.2783>.
- [6] T. Eschenhagen, L. Carrier, Cardiomyopathy phenotypes in human-induced pluripotent stem cell-derived cardiomyocytes—a systematic review, *Pflug. Arch. Eur. J. Physiol.* 471 (2019) 755–768, <https://doi.org/10.1007/s00424-018-2214-0>.
- [7] J. Deinsberger, D. Reisinger, B. Weber, Global trends in clinical trials involving pluripotent stem cells: a systematic multi-database analysis, *NPJ Regenerative Medicine* 5 (2020), <https://doi.org/10.1038/s41536-020-00100-4>.
- [8] U. Martin, Therapeutic application of pluripotent stem cells: challenges and risks, *Front. Med.* 4 (2017) 229, <https://doi.org/10.3389/fmed.2017.00229>.
- [9] M. Mandai, Y. Kurimoto, M. Takahashi, Autologous induced stem-cell-derived retinal cells for macular degeneration, *N. Engl. J. Med.* 377 (2017) 792–793, <https://doi.org/10.1056/NEJMc1706274>.
- [10] C. Kropp, D. Massai, R. Zweigerdt, Progress and challenges in large-scale expansion of human pluripotent stem cells, *Process Biochem.* 59 (2017) 244–254, <https://doi.org/10.1016/j.procbio.2016.09.032>.
- [11] F. Manstein, K. Ullmann, C. Kropp, C. Halloin, W. Triebert, A. Franke, C.-M. Farr, A. Sahabian, A. Haase, Y. Breitzkreuz, M. Peitz, O. Brüstle, S. Kalies, U. Martin, R. Olmer, R. Zweigerdt, High density bioprocessing of human pluripotent stem cells by metabolic control and in silico modeling, *Stem cells translational medicine* 10 (2021) 1063–1080, <https://doi.org/10.1002/sctm.20-0453>.
- [12] P. Gupta, M.Z. Ismail, P.J. Verma, A. Fouras, S. Jadhav, J. Bellare, K. Hourigan, Optimization of agitation speed in spinner flask for microcarrier structural integrity and expansion of induced pluripotent stem cells, *Cytotechnology* (2014), <https://doi.org/10.1007/s10616-014-9750-z>.
- [13] A. Sahabian, M. Sgoddia, O. Naujok, R. Dettmer, J. Dahlmann, F. Manstein, T. Cantz, R. Zweigerdt, U. Martin, R. Olmer, Chemically-defined, xeno-free, scalable production of hPSC-derived definitive endoderm aggregates with multilineage differentiation potential, *Cells* 8 (2019), <https://doi.org/10.3390/cells8121571>.

- [14] C.-Y. Huang, C.-L. Liu, C.-Y. Ting, Y.-T. Chiu, Y.-C. Cheng, M.W. Nicholson, P.C. H. Hsieh, Human iPSC banking: barriers and opportunities, *J. Biomed. Sci.* 26 (2019) 87, <https://doi.org/10.1186/s12929-019-0578-x>.
- [15] T. Miyazaki, H. Suemori, Slow cooling cryopreservation optimized to human pluripotent stem cells, *Adv. Exp. Med. Biol.* 951 (2016) 57–65, https://doi.org/10.1007/978-3-319-45457-3_5.
- [16] T. Miyazaki, N. Nakatsuji, H. Suemori, Optimization of slow cooling cryopreservation for human pluripotent stem cells, *Genesis* 52 (2014) 49–55, <https://doi.org/10.1002/dvg.22725>.
- [17] A. Khalili, M. Ahmad, A review of cell adhesion studies for biomedical and biological applications, *Int. J. Math. Stat.* 16 (2015) 18149–18184, <https://doi.org/10.3390/ijms160818149>.
- [18] S. Mollamohammadi, A. Taei, M. Pakzad, M. Totonchi, A. Seifinejad, N. Masoudi, H. Baharvand, A simple and efficient cryopreservation method for feeder-free dissociated human induced pluripotent stem cells and human embryonic stem cells, *Hum. Reprod.* 24 (2009) 2468–2476, <https://doi.org/10.1093/humrep/dep244>.
- [19] K. Watanabe, M. Ueno, D. Kamiya, A. Nishiyama, M. Matsumura, T. Wataya, J. B. Takahashi, S. Nishikawa, K. Muguruma, Y. Sasai, A ROCK inhibitor permits survival of dissociated human embryonic stem cells, *Nat. Biotechnol.* 25 (2007) 681–686, <https://doi.org/10.1038/nbt1310>.
- [20] L. Bahari, A. Bein, V. Yashunsky, I. Braslavsky, Directional freezing for the cryopreservation of adherent mammalian cells on a substrate, *PLoS One* 13 (2018), e0192265, <https://doi.org/10.1371/journal.pone.0192265>.
- [21] A. Bissoyi, K. Pramanik, N.N. Panda, S.K. Sarangi, Cryopreservation of hMSCs seeded silk nanofibers based tissue engineered constructs, *Cryobiology* 68 (2014) 332–342, <https://doi.org/10.1016/j.cryobiol.2014.04.008>.
- [22] Y.A. Petrenko, A.Y. Petrenko, I. Martin, D. Wendt, Perfusion bioreactor-based cryopreservation of 3D human mesenchymal stromal cell tissue grafts, *Cryobiology* 76 (2017) 150–153, <https://doi.org/10.1016/j.cryobiol.2017.04.001>.
- [23] G.M. Fahy, B. Wovk, Principles of cryopreservation by vitrification, *Methods Mol. Biol.* 1257 (2015) 21–82, https://doi.org/10.1007/978-1-4939-2193-5_2.
- [24] G. Bhakta, K.H. Lee, R. Magalhães, F. Wen, S.S. Gouk, D.W. Hutmacher, L. L. Kuleshova, Cryopreservation of alginate-fibrin beads involving bone marrow derived mesenchymal stromal cells by vitrification, *Biomaterials* 30 (2009) 336–343, <https://doi.org/10.1016/j.biomaterials.2008.09.030>.
- [25] K. Wingate, W. Bonani, Y. Tan, S.J. Bryant, W. Tan, Compressive elasticity of three-dimensional nanofiber matrix directs mesenchymal stem cell differentiation to vascular cells with endothelial or smooth muscle cell markers, *Acta Biomater.* 8 (2012) 1440–1449, <https://doi.org/10.1016/j.actbio.2011.12.032>.
- [26] T. Miyazaki, H. Suemori, Cryopreservation of human pluripotent stem cells: a general protocol, *Methods Mol. Biol.* 1235 (2015) 97–104, https://doi.org/10.1007/978-1-4939-1785-3_9.
- [27] J.C. Neubauer, A.F. Beier, N. Geijsen, H. Zimmermann, Efficient cryopreservation of human pluripotent stem cells by surface-based vitrification, *Methods Mol. Biol.* 1257 (2015) 321–328, https://doi.org/10.1007/978-1-4939-2193-5_13.
- [28] H. Zimmermann, F. Wahlsich, C. Baier, M. Westhoff, R. Reuss, D. Zimmermann, M. Behringer, F. Ehrhart, A. Katsen-Globa, C. Giese, U. Marx, V.L. Sukhorukov, J. A. Vasquez, P. Jakob, S.G. Shirley, U. Zimmermann, Physical and biological properties of barium cross-linked alginate membranes, *Biomaterials* 28 (2007) 1327–1345, <https://doi.org/10.1016/j.biomaterials.2006.11.032>.
- [29] H. Zimmermann, F. Ehrhart, D. Zimmermann, K. Müller, A. Katsen-Globa, M. Behringer, P.J. Feilen, P. Gessner, G. Zimmermann, S.G. Shirley, M.M. Weber, J. Metzke, U. Zimmermann, Hydrogel-based encapsulation of biological, functional tissue: fundamentals, technologies and applications, *Appl. Phys. A* 89 (2007) 909–922, <https://doi.org/10.1007/s00339-007-4270-8>.
- [30] M.M. Gepp, B. Fischer, A. Schulz, J. Döbringer, L. Gentile, J.A. Vásquez, J. C. Neubauer, H. Zimmermann, Bioactive surfaces from seaweed-derived alginates for the cultivation of human stem cells, *J. Appl. Phycol.* 29 (2017) 2451–2461, <https://doi.org/10.1007/s10811-017-1130-6>.
- [31] L. Parmegiani, A. Accorsi, G.E. Cognigni, S. Bernardi, E. Troilo, M. Filicori, Sterilization of liquid nitrogen with ultraviolet irradiation for safe vitrification of human oocytes or embryos, *Fertil. Steril.* 94 (2010) 1525–1528, <https://doi.org/10.1016/j.fertnstert.2009.05.089>.
- [32] M. Richards, C.Y. Fong, S. Tan, W.K. Chan, A. Bongso, An efficient and safe xenofree cryopreservation method for the storage of human embryonic stem cells, *Stem Cell.* 22 (2004) 779–789, <https://doi.org/10.1634/stemcells.22-5-779>.
- [33] A. Kreiner, F. Stracke, H. Zimmermann, On the assessment of the stability of vitrified cryo-media by differential scanning calorimetry: a new tool for biobanks to derive standard operating procedures for storage, access and transport, *Cryobiology* 89 (2019) 26–34, <https://doi.org/10.1016/j.cryobiol.2019.06.002>.
- [34] A. Bissoyi, K. Pramanik, Role of the apoptosis pathway in cryopreservation-induced cell death in mesenchymal stem cells derived from umbilical cord blood, *Biopreserv. Biobanking* 12 (2014) 246–254, <https://doi.org/10.1089/bio.2014.0005>.
- [35] A.D. Katsen, B. Vollmar, P. Mestres-Ventura, M.D. Menger, Cell surface and nuclear changes during TNF- α -induced apoptosis in WEHI 164 murine fibrosarcoma cells. A correlative light, scanning, and transmission electron microscopic study, *Virchows Arch.* 433 (1998) 75–83, <https://doi.org/10.1007/s004280050219>.
- [36] A. Katsen-Globa, I. Meiser, Y.A. Petrenko, R.V. Ivanov, V.I. Lozinsky, H. Zimmermann, A.Y. Petrenko, Towards ready-to-use 3-D scaffolds for regenerative medicine, *J. Mater. Sci. Mater. Med.* 25 (2014) 857–871, <https://doi.org/10.1007/s10856-013-5108-x>.
- [37] A. Katsen-Globa, N. Puetz, M.M. Gepp, J.C. Neubauer, H. Zimmermann, Study of SEM preparation artefacts with correlative microscopy, *Scanning* 38 (2016) 625–633, <https://doi.org/10.1002/sca.21310>.
- [38] M. Desouza, P.W. Gunning, J.R. Stehn, The actin cytoskeleton as a sensor and mediator of apoptosis, *BioArchitecture* 2 (2012) 75–87, <https://doi.org/10.4161/bioa.20975>.
- [39] R. Malpique, F. Ehrhart, A. Katsen-Globa, H. Zimmermann, P.M. Alves, Cryopreservation of adherent cells, *Tissue Engineering, Part C, Methods* 15 (2009) 373–386, <https://doi.org/10.1089/ten.tec.2008.0410>.
- [40] A. Schulz, M.M. Gepp, F. Stracke, H. von Briesen, J.C. Neubauer, H. Zimmermann, Tyramine-conjugated alginate hydrogels as a platform for bioactive scaffolds, *J. Biomed. Mater. Res.* 107 (2019) 114–121, <https://doi.org/10.1002/jbm.a.36538>.
- [41] C.J. Hunt, Cryopreservation of human stem cells for clinical application, *Transfusion medicine and hemotherapy* offizielles Organ der Deutschen Gesellschaft für Transfusionsmedizin und Immunhamatologie 38 (2011) 107–123, <https://doi.org/10.1159/000326623>.
- [42] Y. Li, T. Ma, Bioprocessing of cryopreservation for large-scale banking of human pluripotent stem cells, *BioResearch Open Access* 1 (2012) 205–214, <https://doi.org/10.1089/biores.2012.0224>.
- [43] J. Kaindl, I. Meiser, J. Majer, A. Sommer, F. Krach, A. Katsen-Globa, J. Winkler, H. Zimmermann, J.C. Neubauer, B. Winner, Zooming in on Cryopreservation of hPSCs and Neural Derivatives, *Stem Cells Translational Medicine*, 2018, <https://doi.org/10.1002/sctm.18-0121>.
- [44] M.K. Höffding, P. Hyttel, Ultrastructural visualization of the Mesenchymal-to-Epithelial Transition during reprogramming of human fibroblasts to induced pluripotent stem cells, *Stem Cell Res.* 14 (2015) 39–53, <https://doi.org/10.1016/j.scr.2014.11.003>.
- [45] S.M. Frisch, R.A. Sreaton, Anoiaks mechanisms, *Curr. Opin. Cell Biol.* 13 (2001) 555–562, [https://doi.org/10.1016/S0955-0674\(00\)00251-9](https://doi.org/10.1016/S0955-0674(00)00251-9).
- [46] Y. Zhang, X. Chen, C. Gueydan, J. Han, Plasma membrane changes during programmed cell deaths, *Cell Res.* 28 (2018) 9–21, <https://doi.org/10.1038/cr.2017.133>.
- [47] B.C. Heng, C.P. Ye, H. Liu, W.S. Toh, A.J. Rufaihah, Z. Yang, B.H. Bay, Z. Ge, H. W. Ouyang, E.H. Lee, T. Cao, Loss of viability during freeze-thaw of intact and adherent human embryonic stem cells with conventional slow-cooling protocols is predominantly due to apoptosis rather than cellular necrosis, *J. Biomed. Sci.* 13 (2006) 433–445, <https://doi.org/10.1007/s11373-005-9051-9>.
- [48] S.Y. Tee, J. Fu, C.S. Chen, P.A. Janney, Cell shape and substrate rigidity both regulate cell stiffness, *Biophys. J.* 100 (2011) L25–L27, <https://doi.org/10.1016/j.bpj.2010.12.3744>.
- [49] F.C.K. Tan, K.H. Lee, S.S. Gouk, R. Magalhaes, A. Poonepalli, M.P. Hande, G. S. Dawe, L.L. Kuleshova, Optimization of cryopreservation of stem cells cultured as neurospheres: comparison between vitrification, slow-cooling and rapid cooling freezing protocols, *Cryo-Letters* 28 (2007) 445–460. PMID: 18183325.
- [50] T.H. Jang, S.C. Park, J.H. Yang, J.Y. Kim, J.H. Seok, U.S. Park, C.W. Choi, S.R. Lee, J. Han, Cryopreservation and its clinical applications, *Integrative Medicine Research* 6 (2017) 12–18, <https://doi.org/10.1016/j.imr.2016.12.001>.
- [51] P. Mazur, Principles of cryobiology, in: B.J. Fuller, N. Lane, E.E. Benson (Eds.), *Life in the Frozen State*, CRC Press, Boca Raton, FL, 2004, pp. 3–65. <https://www.taylorfrancis.com/chapters/edit/10.1201/9780203647073-10/principles-cryobiology-peter-mazur>.
- [52] N. Manuchehrabadi, Z. Gao, J. Zhang, H.L. Ring, Q. Shao, F. Liu, M. McDermott, A. Fok, Y. Rabin, K.G.M. Brockbank, M. Garwood, C.L. Haynes, J.C. Bischof, Improved tissue cryopreservation using inductive heating of magnetic nanoparticles, *Sci. Transl. Med.* 9 (2017), <https://doi.org/10.1126/scitranslmed.aah4586>.
- [53] A. Ito, K. Yoshioka, S. Masumoto, K. Sato, Y. Hatae, T. Nakai, T. Yamazaki, M. Takahashi, S. Tanoue, M. Horie, Magnetic heating of nanoparticles as a scalable cryopreservation technology for human induced pluripotent stem cells, *Sci. Rep.* 10 (2020) 13605, <https://doi.org/10.1038/s41598-020-70707-6>.
- [54] H. Lv, H. Wang, Z. Zhang, W. Yang, W. Liu, Y. Li, L. Li, Biomaterial stiffness determines stem cell fate, *Life Sci.* 178 (2017) 42–48, <https://doi.org/10.1016/j.lfs.2017.04.014>.
- [55] Y. Wu, F. Wen, S.S. Gouk, E.H. Lee, L.L. Kuleshova, Cryopreservation strategy for tissue engineering constructs consisting of human mesenchymal stem cells and hydrogel biomaterials, *Cryo-Letters* 36 (2015) 325–335. PMID: 26574680.
- [56] V. Mutsenko, S. Knaack, L. Lauterboeck, D. Tarusin, B. Sydykov, R. Cabiscol, D. Ivnev, J. Belikan, A. Beck, D. Dipresa, A. Lode, T. El Khassawna, M. Kampschulte, R. Scharf, A.Y. Petrenko, S. Korossis, W.F. Wolkers, M. Gelinsky, B. Glasmacher, O. Gryshkov, Effect of ‘in air’ freezing on post-thaw recovery of Callithrix jacchus mesenchymal stromal cells and properties of 3D collagen-hydroxyapatite scaffolds, *Cryobiology* 92 (2020) 215–230, <https://doi.org/10.1016/j.cryobiol.2020.01.015>.
- [57] S. Hong, E. Ergezen, R. Lec, K.A. Barbee, Real-time analysis of cell-surface adhesive interactions using thickness shear mode resonator, *Biomaterials* 27 (2006) 5813–5820, <https://doi.org/10.1016/j.biomaterials.2006.07.031>.
- [58] B.M. Gumbiner, Cell adhesion, *Cell* 84 (1996) 345–357, [https://doi.org/10.1016/S0092-8674\(00\)81279-9](https://doi.org/10.1016/S0092-8674(00)81279-9).
- [59] A.E. Carlsson, Actin dynamics: from nanoscale to microscale, *Annu. Rev. Biophys.* 39 (2010) 91–110, <https://doi.org/10.1146/annurev.biophys.093008.131207>.
- [60] V. Ragoonanan, A. Hubel, A. Aksan, Response of the cell membrane-cytoskeleton complex to osmotic and freeze/thaw stresses, *Cryobiology* 61 (2010) 335–344, <https://doi.org/10.1016/j.cryobiol.2010.10.160>.
- [61] V. Ragoonanan, R. Less, A. Aksan, Response of the cell membrane-cytoskeleton complex to osmotic and freeze/thaw stresses, *Part 2, Cryobiology* 66 (2013) 96–104, <https://doi.org/10.1016/j.cryobiol.2012.10.008>.
- [62] P. Mazur, S.P. Leibo, E. Chu, A two-factor hypothesis of freezing injury, *Exp. Cell Res.* 71 (1972) 345–355, [https://doi.org/10.1016/0014-4827\(72\)90303-5](https://doi.org/10.1016/0014-4827(72)90303-5).

- [63] T.D. Pollard, R.D. Goldman, Overview of the cytoskeleton from an evolutionary perspective, *Cold Spring Harbor perspectives in biology* 10 (2018), <https://doi.org/10.1101/cshperspect.a030288>.
- [64] B. Graham, T.L. Bailey, J.R.J. Healey, M. Marcellini, S. Deville, M.I. Gibson, Polyproline as a minimal antifreeze protein mimic that enhances the cryopreservation of cell monolayers, *Angew. Chem.* 56 (2017) 15941–15944, <https://doi.org/10.1002/anie.201706703>.
- [65] E. Kondo, K. Wada, K. Hosokawa, M. Maeda, Cryopreservation of adhered mammalian cells on a microfluidic device: toward ready-to-use cell-based experimental platforms, *Biotechnol. Bioeng.* 113 (2016) 237–240, <https://doi.org/10.1002/bit.25704>.
- [66] H. Ohkawara, S. Miyagawa, S. Fukushima, S. Yajima, A. Saito, H. Nagashima, Y. Sawa, Development of a vitrification method for preserving human myoblast cell sheets for myocardial regeneration therapy, *BMC Biotechnol.* 18 (2018) 56, <https://doi.org/10.1186/s12896-018-0467-5>.
- [67] R.J. de Vries, P.D. Banik, S. Nagpal, L. Weng, S. Ozer, T.M. van Gulik, M. Toner, S. N. Tessier, K. Uygun, Bulk droplet vitrification: an approach to improve large-scale hepatocyte cryopreservation outcome, *Langmuir the ACS journal of surfaces and colloids* 35 (2019) 7354–7363, <https://doi.org/10.1021/acs.langmuir.8b02831>.